Altering the electronic properties of diamondoids through encapsulating small particles

2009 J. Phys.: Condens. Matter 21 215303

(http://iopscience.iop.org/0953-8984/21/21/215303)

J. Phys.: Condens. Matter **21** (2009) 215303 (8pp) doi:10.1088/0953-8984/21/21/215303

Altering the electronic properties of diamondoids through encapsulating small particles

Farah Marsusi[1] **and Kavoos Mirabbaszadeh**[1,2]

[1] Department of Physics, Amirkabir University of Technology, PO Box 15875-4413, Tehran, Iran
[2] Nanotechnology Research Center, Amirkabir University of Technology, PO Box 15875-4413, Tehran, Iran

E-mail: mirabbas@aut.ac.ir

Received 24 September 2008, in final form 1 March 2009
Published 1 May 2009
Online at stacks.iop.org/JPhysCM/21/215303

Abstract

The stability, optimized structure, and electronic gap of four diamondoid complexes, adamantane, $C_{10}H_{16}$, diamantane, $C_{14}H_{20}$, triamantane, $C_{18}H_{24}$ and the T_d-symmetry isomer of pentamantane, $C_{26}H_{32}$, incorporating cage-centered small atoms and ions (X@cage, where X = H^+, $Li^{0,+}$, $Be^{0,+,2+}$, $Na^{0,+}$, $Mg^{0,2+}$, He, Ne, and F^-) have been studied at the B3LYP hybrid level of theory. All adamantane complexes, except those encapsulating H^+ and Mg, are endohedral minima. In contrast no diamantane complexes are minima. A wide variety of atoms and ions can be encapsulated by triamantane and pentamantane molecules. The complexes are more stable for smaller and more highly charged metallic guest species. The electronic HOMO–LUMO gaps of diamondoid complexes are significantly affected by the inclusion of charged particles. The stability of the structures, the amount of the charges which are transferred between small particles and diamondoids cages, and the change in the HOMO–LUMO gaps of diamondoids are nearly the same for the corresponding possible complexes. All these features mostly depend on the charge, the size and the type of the encapsulated particle, and not on the type of diamondoid.

(Some figures in this article are in colour only in the electronic version)

S Supplementary data are available from stacks.iop.org/JPhysCM/21/215303

1. Introduction

Designing nano-scale building blocks and engineering their optoelectronic properties is one of the most rapidly evolving fields of nanomaterials. The recognition of diamondoids and their derivatives as suitable building blocks for nanotechnological devices has sparked an interest in both calculating and measuring their optoelectronic properties [1]. The interest in these molecules comes from both pure and applied science. Given that diamondoids are nano-sized hydrogen terminated diamond fragments, it was anticipated that reducing the size of diamond to the nano-scale would have a strong effect on its optical gap. According to the quantum confinement (QC) model, with decreasing particle size the energy gap between the lowest unoccupied molecular orbital (LUMO) and the highest occupied molecular orbital (HOMO) increases. Experimentally, Si and Ge nanocrystals with sizes above 1 nm exhibit clear, theoretically confirmed QC effects [2, 3]. Bulk diamond has a large band gap, so it is expected that the HOMO–LUMO energy gap of diamondoids will be pushed further into the UV range. This could be applied in a new generation of UV sensors. Consequently, many recent theoretical and experimental studies have been performed to investigate the optoelectronic properties of these molecules [4–7]. However, diffusion quantum Monte Carlo (DMC) [7], along with density functional theory (DFT) calculations with both plane-wave and diffuse Gaussian basis sets [4, 7], show that, in contrast to Si and Ge nanoclusters, QC effects disappear in diamondoids larger than 1 nm. According to [4] and [7], for a diamond nanoparticle larger than 1 nm, the HOMO–LUMO energy gap is even smaller than the gap of

bulk diamond. This result has been confirmed by further experimental investigation of the soft x-ray absorption and emission spectra [8, 9]. The spectra from x-ray absorption spectroscopy (XAS) show that diamondoids exhibit negligible shifting in the LUMO levels and the changes in HOMO–LUMO energy gap stem only from QC effects in the HOMO levels. Therefore diamondoids do not seem likely to be as useful as was earlier predicted for UV sensor applications. One possible way of overcoming this problem is to use diamondoid derivatives. First-principles studies of the three groups of diamondoid complexes and their derivatives have shown that when residues like Na are added, their electronic properties, such as the HOMO–LUMO gap or the electrical conductance, can be changed. It has also been demonstrated that the quantum conductance of diamondoid molecules and their derivatives changes significantly when their orientations are changed [10]. This has given rise to a new branch of materials for application in nano-electro-mechanical systems and micro-electro-mechanical systems. On the other hand, it has also been shown that incorporating charged species into silicon fullerene clusters enables their optoelectronic properties to be tuned [11–13]. This motivated us to explore another idea: whether the encapsulation of small ions in the diamondoid cages could yield stable diamondoid complexes (X@cage, where X = H^+, $Li^{0,+}$, $Be^{0,+,2+}$, $Na^{0,+}$, $Mg^{0,2+}$, He, Ne, and F^-), and whether this would affect the electronic properties of these nanostructures. To answer this question we have performed theoretical calculations using the DFT method for four diamondoids: adamantane ($C_{10}H_{16}$), diamantane ($C_{14}H_{20}$), triamantane ($C_{18}H_{24}$) and finally a T_d-symmetry isomer of pentamantane ($C_{26}H_{32}$). Adamantane, diamantane, and triamantane belong to the T_d, D_{3d} and C_{2v} point groups, respectively. We have investigated the effect of encapsulating different small cage-centered endohedral particles on the stability and electronic gap of these molecules. We have sought to find how the HOMO–LUMO energy gap of diamondoid complexes changes as a function of the size and symmetry of the molecules, and also the size, charge, and type of the guest particles. According to our DFT results, it is possible to include some small particles at the T_d and C_{2v} center of diamondoids. Our studies have also shown that, unlike diamantane, the complexes with T_d and C_{2v} symmetry comprise endohedral minima. We have furthermore deduced that in comparison to Si nanoclusters [14], although diamondoids do not show significant QC effects [4, 7], they are much more sensitive to interaction of their cages with encapsulated charged particles. The stabilities of the endohedral minima of diamondoids have been evaluated by comparing their energies (E_{endo}) to the sum of the energies of their isolated components. Our results demonstrate that in molecules with T_d or C_{2v} symmetries, the stability of the encapsulated complex is greatest for small, highly charged metallic particles such as Be^{2+}. The calculated natural charges indicate that a significant amount of electronic charge density is transferred between the cage's atoms and the central particle. This results in a Coulomb interaction between the cage and the encapsulated particle, and also polarizes the complex, thereby altering the electronic properties of diamondoids considerably. However, because the interaction between a charged guest particle and its host is greatest when the host molecule is small, the introduction of a guest particle has the most significant effect on the HOMO–LUMO gap of the smallest diamondoid complex, $X@C_{10}H_{16}$. Our calculations show that, for different diamondoids, in addition to charge-transfer, the trends of the stability and the trends of the variation in the HOMO–LUMO gap are nearly the same.

Table 1. DFT-calculated HOMO–LUMO gap of three diamondoids at various XC functionals in comparison with DMC optical gaps, all in eV. The trend of electronic gap against size (the diameter of the particle in nm) is the same as DMC for each level of DFT, but the absolute results of B3LYP are closer to the high accuracy DMC results.

Molecule	Symmetry	Size	B3LYP	BLYP	PBE	LDA	DMC[a]
Adamantane	T_d	0.50	7.18	5.69	5.77	5.90	7.61
Diamantane	D_{3d}	0.69	6.80	5.34	5.41	5.57	7.32
Pentamantane	T_d	0.74	6.39	5.00	5.04	5.17	7.04

[a] DMC results are taken from [7].

2. Computational methods

Diamondoid complexes were optimized at the B3LYP/6-31G(d, p) level of theory. Vibrational frequency analyses (at the same level) characterized the optimized structures as minima or higher stationary points. All energies were corrected using unscaled zero-point vibrational energies (ZPVE), and the results have also been compared with the non-corrected case. The ZPVE corrected relative energies, ΔE^*, of endohedral complex minima were evaluated by comparing the ZPE corrected of X@cage (E_{endo}) to the sum of the energies of the isolated components, E_{cage} (ZPVE) and E_X ($\Delta E^* = E_{endo} - [E_{cage} + E_X]$). B3LYP is Becke's three-parameter hybrid functional [15], which uses the non-local correlation provided by the LYP expression [16]. The B3LYP functional was chosen because mixing in a fraction of exact exchange leads to the cancelation of self-energy errors. Recently, DFT band gap calculations using the B3LYP functional have been proposed as a relatively computationally inexpensive alternative to many-body methods such as coupled cluster, GW-Bethe Salpeter (GW-BSE), and quantum Monte Carlo (QMC). It has also been shown that B3LYP can predict qualitatively correct trends in the optical gap of a given structure as a function of size [17, 18]. We have also shown in table 1, that the B3LYP-predicted HOMO–LUMO gaps of three diamondoids are in much better agreement with accurate DMC optical gaps taken from [7] than those predicted using other functionals. The 6-31G [19] basis set was used and additional flexibility was built in by adding higher angular momentum basis functions. Since the highest angular momentum orbital for hydrogen and carbon are s and p states, respectively, the polarizations of the atoms were described by adding sets of p and d functions. According to [7], the LUMO in diamondoids is a delocalized state with a considerable charge outside of the H atoms terminating the surface. So it is advantageous to augment the basis set with diffuse functions, i.e. functions that have smaller orbital exponents than those normally used. Concern for this characteristic behavior of diamondoids is particularly important for the investigation of properties which

Table 2. The corrected ZPVE at B3LYP/6-31++G(d, p) level for adamantane complexes (E_{endo}), small charged particles (E_X), relative energy (ΔE^*), the non-corrected ZPVE relative energy (ΔE), and the number of imaginary frequencies (N_{Imag}). The corrected ZPVE of total energy of the single cage at this level is −390.5114 (au).

X@$C_{10}H_{16}$	E_{endo} (au)	E_X (au)	ΔE^* (eV)	ΔE (eV)	N_{Imag}
Li^+@$C_{10}H_{16}$	−397.6990	−7.2846	2.64	2.54	0
Be^{2+}@$C_{10}H_{16}$	−404.5340	−13.6523	−10.08	−10.10	0
Na^+@$C_{10}H_{16}$	−552.1369	−162.0812	12.40	12.66	0
Mg^{2+}@$C_{10}H_{16}$	−589.6354	−199.2274	2.82	3.06	0
F^-@$C_{10}H_{16}$	−489.7910	−99.8597	15.78	16.49	0

Table 3. The corrected ZPVE at B3LYP/6-31G(d, p) level for adamantane complexes (E_{endo}), small charged particles (E_X), relative energy (ΔE^*), the non-corrected ZPVE relative energy (ΔE), the number of imaginary frequencies (N_{Imag}), and the charge on the guest species. The corrected ZPVE of total energy of the single cage at this level is −390.5036 (au).

X@$C_{10}H_{16}$	E_{endo} (au)	E_X (au)	ΔE^* (eV)	ΔE (eV)	N_{Imag}	Charge@X
Li@$C_{10}H_{16}$	−397.7651	−7.4910	6.24	6.26	0	0.15
Li^+@$C_{10}H_{16}$	−397.6928	−7.2845	2.59	2.51	0	0.71
Be@$C_{10}H_{16}$	404.8141	−14.6684	9.74	10.47	0	0.45
Be^+@$C_{10}H_{16}$	−404.7493	−14.3359	2.46	2.87	0	1.27
Be^{2+}@$C_{10}H_{16}$	−404.5322	−13.6522	−10.24	−10.25	0	1.66
Na@$C_{10}H_{16}$	−552.2131	−162.2799	15.52	15.85	0	0.01
Na^+@$C_{10}H_{16}$	−552.1319	−162.0813	12.32	12.60	0	0.75
Mg^{2+}@$C_{10}H_{16}$	−589.6323	−199.2273	2.68	2.94	0	1.73
He@$C_{10}H_{16}$	−393.16511	−2.9070	6.68	6.59	0	0.06
Ne@$C_{10}H_{16}$	−518.8179	−128.8944	15.78	16.14	0	0.03
F^-@$C_{10}H_{16}$	489.7553	−99.7541	13.67	14.39	3	−0.62

are related to the optical gaps of these molecules. However, using diffuse basis sets results in a higher computational cost, especially for larger molecules such as $C_{26}H_{32}$. Our first consideration in the current work is to inspect the order of the stationary points of diamondoid complexes with sufficient accuracy while keeping computational costs to a minimum. For this purpose we have tried two kinds of the Gaussian basis functions: 6-31G(d, p) and diffuse 6-31G++(d, p). We have optimized the geometry of the smallest molecule $C_{10}H_{16}$ using these basis sets, and have compared the results. As shown in tables 2 and 3, with the exception of F^-@$C_{10}H_{16}$, the relative energies deduced from B3LYP/6-31G(d, p), and B3LYP/6-31++G(d, p) calculations are generally in good agreement ($\leqslant$0.16 eV). However, an anomaly is found in the case of the F^-@$C_{10}H_{16}$ complex. The calculations using the 6-31G(d, p) basis set indicate that it has three imaginary frequencies ($N_{Imag} = 3$, triply degenerate at low frequency 57i cm^{-1}). In contrast, by performing calculations with the diffuse basis set, B3LYP/6-31++G(d, p), this diamondoid complex is found to be a stationary minimum point with no imaginary frequencies ($N_{Imag} = 0$). From these tables the difference in relative energy, ΔE^*, using the two basis sets for F^-@$C_{10}H_{16}$ is 2.11 eV. However, as a large, non-metallic anion, F^- is an exception in this study, and no other complex in tables 2 and 3 shows differences in the vibrational frequencies obtained using the two above-mentioned basis sets. Consequently, the inexpensive 6-31G(d, p) basis set was used throughout this work (except for F^-@$C_{10}H_{16}$) to optimize the geometry of the complex to calculate the vibrational frequencies. The optimized endohedral complexes were used to calculate HOMO–LUMO gaps at the B3LYP/6-31++G(d, p) level and the natural bond orbitals (NBO) [20]. The outcomes of the calculations were utilized to construct orbital interaction diagrams. All calculations were performed using the Gaussian 98 code [21]. Absolute energies, ZPVE, and optimized endohedral standard orientations are summarized in the supporting information (available at stacks.iop.org/JPhysCM/21/215303).

3. Results and discussion

3.1. Stability of the diamondoid-complex structures

Through analyses of the vibrational frequencies, it has been determined that the stationary point is sensitive to the symmetry of the cage, and also to the type and size of the small ion. The adamantane, triamantane, and pentamantane molecules are good host cages, because the majority of the related endohedral complexes are minima (see figure 1 and also tables 2–5). However, for all diamondoids in our study, H^+@ cages and Mg@cages are unstable with $N_{Imag} \geqslant 1$ (triply degenerate imaginary frequency at 1397i cm^{-1}, and 1313i cm^{-1} for H^+@$C_{10}H_{16}$ and H^+@$C_{26}H_{32}$ complexes, and one at 960i cm^{-1} for H^+@$C_{18}H_{24}$, respectively).

For D_{3d} symmetric $C_{14}H_{20}$, all the resulting complexes are higher order stationary points with $N_{Imag} \geqslant 1$.

In spite of its small size, the majority of the particles in our study ($Li^{0,+}$, $Be^{0,+,2+}$, $Na^{0,+}$, Mg^{2+}, He, Ne, F^-) can be encapsulated by T_d symmetric adamantane. The HOMO and LUMO of some adamantane complexes and a simple cage for comparison are shown in figure 2. The most stable complex, Be^{2+}@$C_{10}H_{16}$, has the most similar HOMO and LUMO isosurface to the corresponding isosurface of the single cage. The HOMO isosurface plots of the complexes

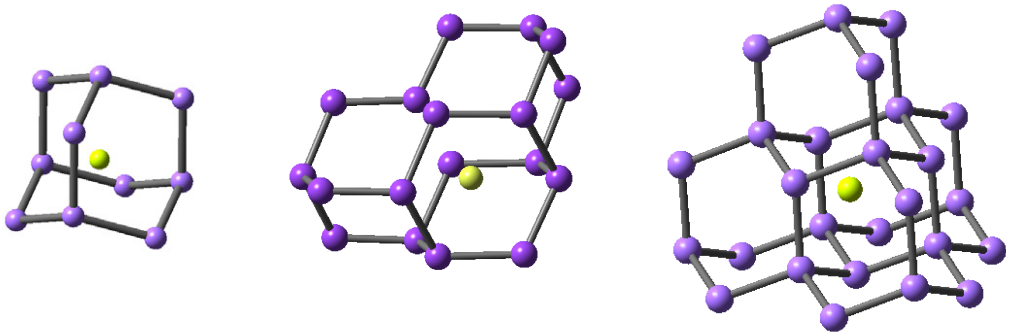

Figure 1. Structure of $X@C_{10}H_{16}$, $X@C_{18}H_{24}$, and $X@C_{26}H_{32}$.

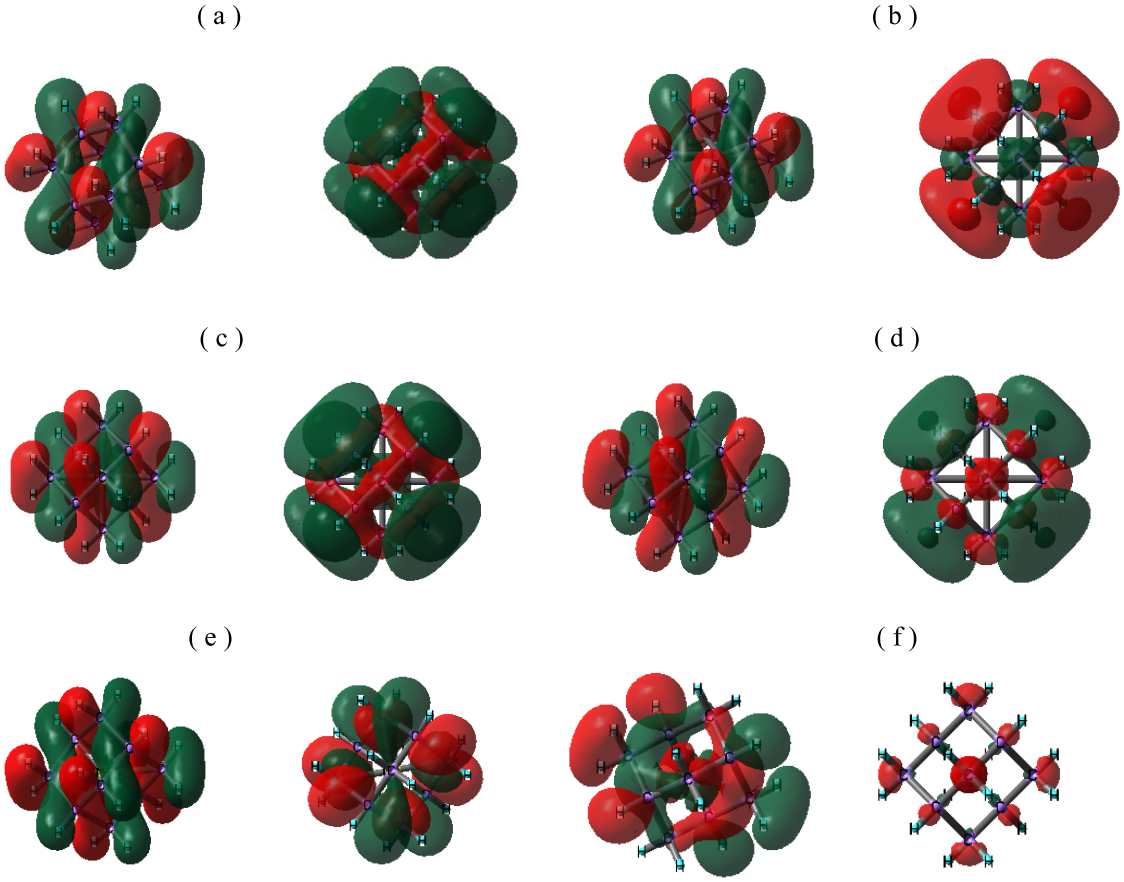

Figure 2. The HOMO (left) and LUMO (right) isosurface plots of adamantane and $X@C_{10}H_{16}$ complexes. (a) $C_{10}H_{16}$. (b) $Li^{+}@C_{10}H_{16}$. (c) $Be^{2+}@C_{10}H_{16}$. (d) $Na^{+}@C_{10}H_{16}$. (e) $Mg^{2+}@C_{10}H_{16}$. (f) $F^{-}@C_{10}H_{16}$.

encapsulating metallic species do not change significantly relative to the HOMO isosurface of the single cage. The LUMO isosurface plot of $Mg^{2+}@C_{10}H_{16}$ is stretched from the hydrogen terminated surface to the cage center, where the relatively large and also highly charged ion is placed. In the case of $F^{-}@C_{10}H_{16}$, both HOMO and LUMO isosurfaces are different relative to the single cage. According to [14], although $F^{-}@Si_{10}H_{16}$ is a stable structure, its LUMO state also differs from $Si_{10}H_{16}$. Therefore we cannot conclude that the instability, which is observed in the structure of $F^{-}@C_{10}H_{16}$, is a consequence of the deformation of its HOMO and LUMO states; however we expect that it should affect some of its chemical properties relative to other complexes.

We have also constructed the orbital interaction diagrams to explain how the stability of the structure relates to the type of the enclosed particle. However, $Be@C_{10}H_{16}$ is a stable structure; figure 3 shows the repulsive four-electron, two-orbital interaction reduces the stability of the complex. This is accompanied by a reduction in the HOMO–LUMO

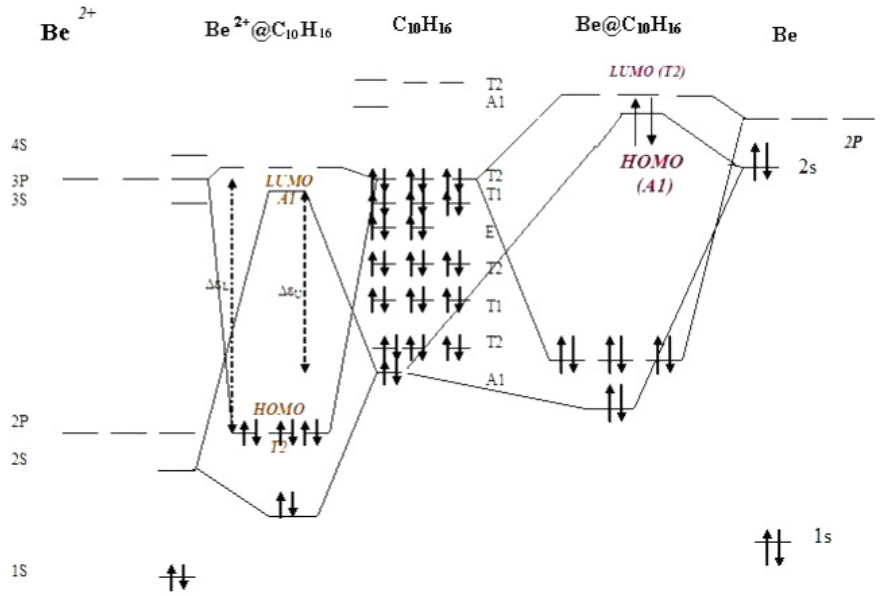

Figure 3. Orbital interaction diagrams for $Be^{0,2+}@C_{10}H_{16}$. The energy interval and symmetries of the levels were obtained from Gaussian 98 NBO output files.

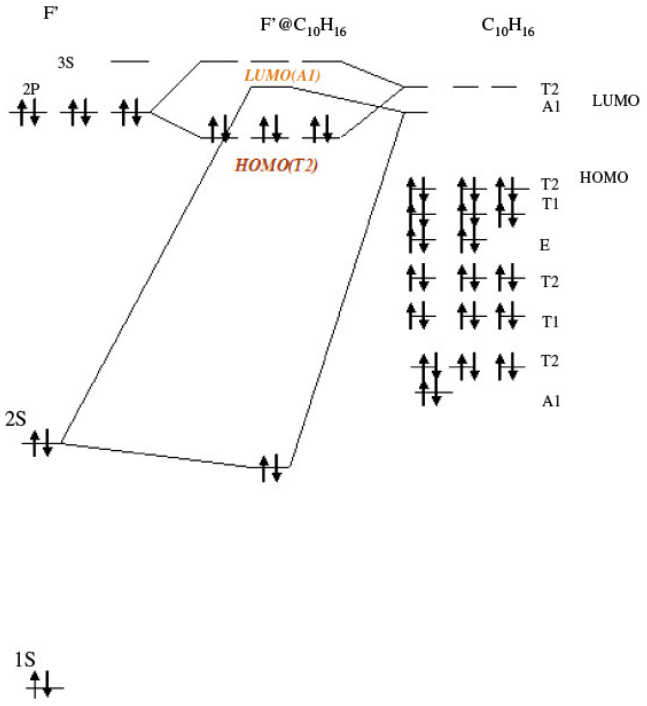

Figure 4. Orbital interaction diagrams for $F-@C_{10}H_{16}$. The energy interval and symmetries of the levels were obtained from Gaussian 98 NBO output files.

gap compared to the simple cage. The interaction of the A_1 symmetric level of $C_{10}H_{16}$ keeps the A_1 orbital of $Be@C_{10}H_{16}$ below the T_2, and ensures that the ground state is a closed shell singlet. In contrast, the positive charge of Be^{2+} lowers all of the adamantane orbitals and increases the stability and the HOMO–LUMO gap. The negative charge of the F^- in figure 4 raises the adamantane orbitals, reduces the stability and reduces the HOMO–LUMO gap.

Triamantane, which consists of three diamond cages and has the chemical formula $C_{18}H_{24}$, belongs to the C_{2v} point group (figure 1). In the geometry optimization of triamantane complexes we have changed the initial position of the central particle by a small amount to find a stationary minimum point with $N_{\mathrm{Imag}} = 0$. In all of the possible structures in table 4 the central particles are not exactly in the center of the molecule. With this method we have found that a wide variety of atoms and ions, including $Li^{0,+}$, Be^{2+}, $Na^{0,+}$, He and Ne, can be enclosed by this molecule. We could not find a suitable initial position for $Be^{0,+}$, which leads to a complex minima, while F^- endohedral complex geometry optimizations failed to converge.

Compared with adamantane, the T_d symmetric isomer of pentamantane with five cages and more electrons can encapsulate fewer species (including $Li^{0,+}$, Be^{2+}, $Na^{0,+}$, Mg^{2+}, He, Ne, F^-, see table 5). It is worth noting that pentamantane is not able to form a cage-centered $Be^{0,+}$ endohedral complex.

From tables 2–5 it can be seen that, as the guest species becomes larger, the ZPVE correction becomes more important to the relative energy. It is predicted that the encapsulation of smaller and more highly charged metallic species at the center of the molecules is the most favorable.

The most stable complex occurs for $X = Be^{2+}$ in all complexes (with $\Delta E^* = -10.24$ eV for $C_{10}H_{16}$, -11.33 eV for $C_{18}H_{24}$, and -12.11 eV for $C_{26}H_{32}$, respectively). Be^{2+} is the smallest metallic charged species in our study. Including neutral Be at the T_d center of the adamantane (table 3) with $\Delta E^* = 9.74$ eV is not as stable as $Be^{2+}@C_{10}H_{16}$. Including the more highly charged, but larger sized, Mg^{2+} ion at the center of adamantane increases the C–C bond length, destabilizing the structure and increasing ΔE^* to 2.68 eV, which is still much more stable than $Be@C_{10}H_{16}$. With the increase of the size of the cage from adamantane (with

Table 4. The corrected ZPVE at the B3LYP/6-31G(d, p) level for triamantane complexes (E_{endo}), small charged particles (E_X), relative energy (ΔE^*), the non-corrected ZPVE relative energy (ΔE), the number of imaginary frequencies (N_{Imag}), and the charge on the guest species. The corrected ZPVE of total energy of the single cage at this level is −700.0689 (au).

X@$C_{18}H_{24}$	E_{endo} (au)	E_X (au)	ΔE^* (eV)	ΔE (eV)	N_{Imag}	ChargeX@
Li@$C_{18}H_{24}$	−707.3284	−7.4910	6.30	6.53	0	0.12
Li^+@$C_{18}H_{24}$	−707.2699	−7.2845	2.28	2.18	0	0.72
Be^{2+}@$C_{18}H_{24}$	−714.1375	−13.6522	−11.33	−11.36	0	1.68
Na@$C_{18}H_{24}$	−861.7779	−162.2799	15.53	15.84	0	0.004
Na^+@$C_{18}H_{24}$	−861.7076	−162.0813	12.05	12.28	0	0.76
He@$C_{18}H_{24}$	−702.7286	−2.9070	6.73	6.63	0	0.07
Ne@$C_{18}H_{24}$	−828.3830	−128.8944	15.79	16.10	0	0.04

Table 5. The ZPVE corrected B3LYP/6-31G(d, p) energy of pentamantane complexes (E_{endo}), small charged particles (E_X), relative energy (ΔE^*), the non-corrected ZPVE relative energy (ΔE), the number of imaginary frequencies (N_{Imag}), and the charge on the guest species. The ZPVE corrected total energy of the single cage at this level is −1009.6403 (au).

X@$C_{26}H_{32}$	E_{endo} (au)	E_X (au)	ΔE^* (eV)	ΔE (eV)	N_{Imag}	ChargeX@
Li@$C_{26}H_{32}$	−1016.8897	−7.4910	6.57	6.68	0	0.42
Li^+@$C_{26}H_{32}$	−1016.8483	−7.2845	2.08	2.00	0	0.72
Be^{2+}@$C_{26}H_{32}$	−1023.7375	−13.6522	−12.11	−12.12	0	1.68
Na@$C_{26}H_{32}$	−1171.3405	−162.2799	15.77	16.18	0	−0.05
Na^+@$C_{26}H_{32}$	−1171.2781	−162.0813	12.06	12.36	0	0.79
Mg^{2+}@$C_{26}H_{32}$	−1208.8296	−199.2273	1.03	1.33	0	1.73
He@$C_{26}H_{32}$	−1012.2976	−2.9070	6.80	6.71	0	0.07
Ne@$C_{26}H_{32}$	1137.9448	−128.8944	16.05	16.42	0	0.06
F^-@$C_{26}H_{32}$ ‘	−1108.8905	−99.7541	13.71	14.40	0	−0.64

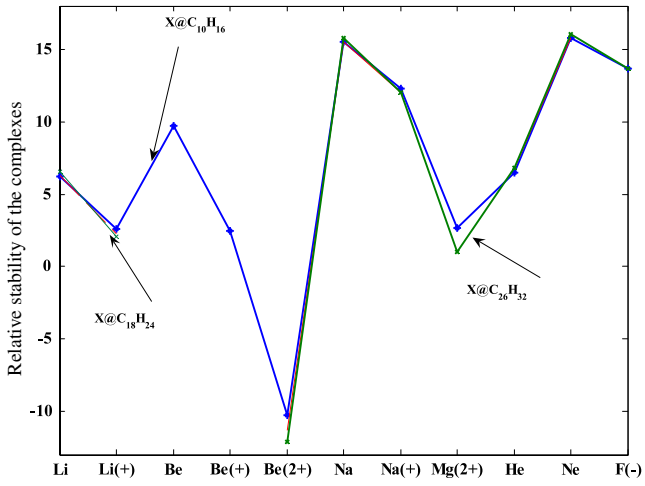

Figure 5. Comparison the stability of X@$C_{10}H_{16}$, X@$C_{18}H_{24}$, and X@$C_{26}H_{32}$ complexes.

diameter 0.50 nm) to pentamantane (with diameter 0.74 nm), this improves to 1.03 eV.

The variations in ΔE^* against different charged particles for three diamondoids are plotted in figure 5, and show a symmetry independent behavior. If a diamondoid complex is a possible structure, its stability will largely depend on the type and charge of the encapsulated particle. It is observed that the trends of variation are the same in adamantane. For those possible triamantane complexes this curve is almost superimposed on the curve of X@$C_{10}H_{16}$ at each point. Moreover, except for $X = F^-$, the complexes become more stable (lower ΔE) as the cage size is increased. This is especially important for highly charged species such as Be^{2+} and Mg^{2+}.

The natural charges in tables 3–5 indicate that a significant amount of electronic charge density has been transferred between the cage atoms and the central particle. Surveying these tables reveals that, independent of the cage, the amount of charge-transfer mostly depends on the type of central particle (only a surprisingly different feature is observed for Li@cage). Some differences in the amounts of the charge-transfer of X@$C_{10}H_{16}$ between the reference [22] and the present study are observed. These are due to the different basis sets which are used in the NBO calculations of the two studies.

3.2. Optimized structures

The optimized C–C and C–H bond lengths for X@cages are summarized in tables 6–8. Reviewing these tables, it is obvious that, compared to the corresponding single cage, the C–C bond lengths of X@$C_{10}H_{16}$, X@$C_{18}H_{24}$ and the inner C–C bond length of X@$C_{26}H_{32}$ have been stretched from their initial values of 1.543 Å, 1.549 Å and 1.553 Å, respectively. Figure 6 shows that an increase in the size of the encapsulated particle implies a greater stretch of the cages. The X@$C_{10}H_{16}$ curve in this figure is in agreement with the corresponding curve of [22]. The donation of electron density from the encapsulated particle into the cages' atoms stretches the bond lengths. For example the C–C bond lengths increase from 1.616 (Be@$C_{10}H_{16}$) to 1.628 Å (Be^{2+}@$C_{10}H_{16}$). This effect is more significant for more highly charged species. However, the stretch of the C–C bonds length in X@ $C_{26}H_{32}$ compresses the C–C bond lengths between one inner carbon and one outer carbon (C–CH_2) from 1.540 Å with increasing encapsulated species size.

Table 6. B3LYP/6-31G** optimized C–C, C–H, and C–X bond lengths of X@$C_{10}H_{16}$ in Å, and at the B3LYP/6-31G(d, p) level of theory (for F^-@$C_{10}H_{16}$ the diffuse basis set was used). C(H), and C(H_2) represent those carbons which are involved in the C–H and H–C–H antibonding, respectively.

Bond	Single cage	Li@	Li^+@	Be@	Be^+@	Be^{2+}@	Na@	Na^+@	Mg^{2+}@	He@	Ne@	F^-@
C(H_2)–C(H)	1.543	1.616	1.623	1.616	1.621	1.628	1.745	1.751	1.755	1.607	1.735	1.717
C(H)–H	1.097	1.091	1.086	1.125	1.102	1.086	1.089	1.086	1.085	1.098	1.099	1.140
C(H_2)–H	1.098	1.096	1.092	1.115	1.102	1.091	1.094	1.091	1.090	1.097	1.096	1.104
C(H)–X		1.644	1.651	1.645	1.645	1.646	1.795	1.801	1.803	1.623	1.778	1.724
C(H_2)–X		1.849	1.858	1.848	1.856	1.868	1.984	1.990	1.997	1.845		1.979

Table 7. B3LYP/6-31G** optimized C–C, C–H, and C–X bond lengths of X@$C_{18}H_{24}$ in Å, and at the B3LYP/6-31G(d, p) level of theory. The C(H), and C(H_2) represent those carbons which are involved in the C–H and H–C–H antibonding, respectively.

Bond	Single cage	Li@	Li^+@	Be^{2+}@	Na@	Na^+@	He@	Ne@
C(H)–C(H)	1.549	1.615	1.629	1.633	1.745	1.762	1.613	1.746
C(H_2)–(H)	1.537	1.601	1.616	1.615	1.721	1.726	1.602	1.708
C(H)–	1.099	1.096	1.087	1.085	1.092	1.087	1.099	1.100
C(H)–		1.640	1.649		1.799	1.804		1.785

Table 8. B3LYP/6-31G^{**} optimized C–C, C–H, and C–X bond lengths of X@$C_{26}H_{32}$ in Å. C(H), and C(H_2) represent those carbons which are involved in C–H and H–C–H antibonding, respectively.

Bond	Single cage	Li@	Li^+@	Be^{2+}@	Na@	Na^+@	Mg^{2+}@	He@	Ne@	F^-@
C–C(H)	1.553	1.623	1.630	1.636	1.747	1.751	1.757	1.613	1.735	1.716
C–C(H_2)	1.540	1.534	1.536	1.538	1.525	1.529	1.529	1.537	1.529	1.528
C(H)–C(H_2)	1.539	1.543	1.546	1.545	1.558	1.560	1.558	1.547	1.561	1.564
C–X		1.867	1.877	1.892	1.992	1.999	2.011	1.863		
C(H)–X		1.635	1.638	1.631	1.788	1.788	1.787	1.611	1.768	1.715

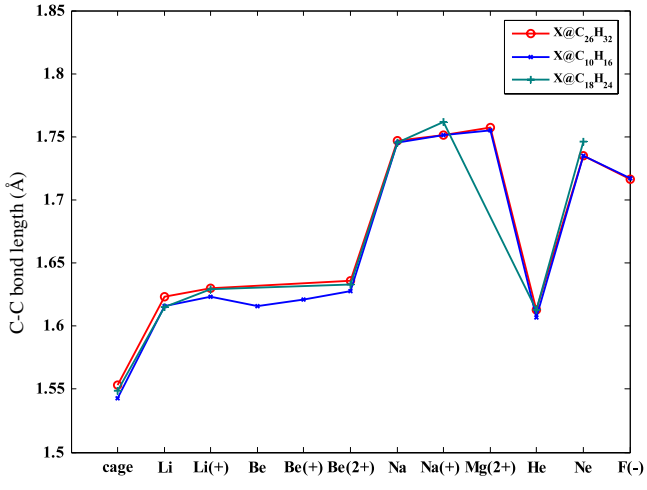

Figure 6. Calculated B3LYP/6-31G(d, p) optimized C–C bond length trends of possible X@$C_{10}H_{16}$, X@$C_{18}H_{24}$, and X@$C_{26}H_{32}$.

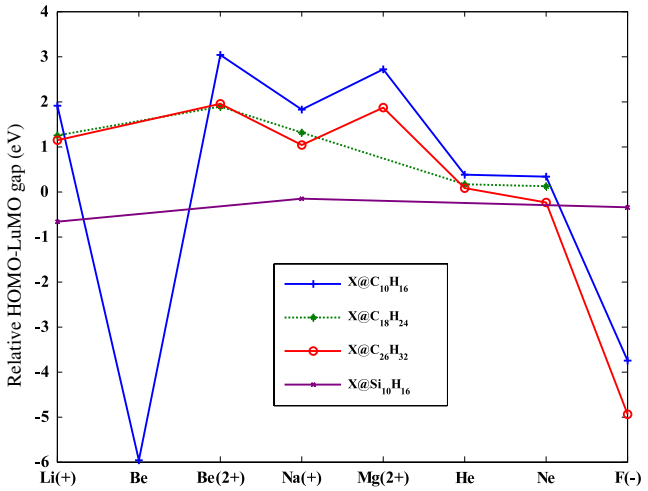

Figure 7. Calculated B3LYP/6-31G(d, p) HOMO–LUMO gaps of possible spin singlet complexes X@$C_{10}H_{16}$, X@$C_{18}H_{24}$, and X@$C_{26}H_{32}$ relative to the corresponding single-cage gaps, along with the relative HOMO–LUMO gap of $Si_{10}H_{16}$ taken from [14].

3.3. HOMO–LUMO gaps

In comparison with Si nanoparticles [14], including charged particles at the centers of diamondoids has a significant effect on their HOMO–LUMO gaps. The interaction of the cage and the charged particle completely changes the calculated gap of the cages. The maximum shifts result from the more highly charged species Be^{2+} (from 7.18 to 10.22 eV in $C_{10}H_{16}$, from 6.58 to 8.46 in $C_{18}H_{24}$, and from 6.39 to 8.35 eV in $C_{26}H_{32}$) and Mg^{2+} (from 7.18 to 8.35 eV in $C_{10}H_{16}$, and from 6.39 to 8.25 eV in $C_{26}H_{32}$). In figure 7 the magnitude of the gap in each complex relative to the corresponding single-cage gap is plotted ([HOMO–LUMO of X@cage]–[HOMO–LUMO of cage]). From this figure, the HOMO–LUMO gap of the smallest diamondoid is more affected by the Coulomb interaction; however the variation in the gaps for all complexes shows the same trend. As expected, the greatest variation in complexes encapsulating metallic species occurs for more

highly charged particles. The relative changes in the HOMO–LUMO gap due to including charged particles at the T_d center of the $Si_{10}H_{16}$ cage from [14] are also added to this figure, and show how much more diamondoid cages are affected by the Coulomb interactions.

4. Conclusion

We have investigated the possibility of including small particles, including ions and atoms, at the center of four diamondoid cages, these being adamantane, $C_{10}H_{16}$ (T_d), diamantane, $C_{14}H_{20}$(D_{3d}), triamantane, $C_{18}H_{24}$(C_{2v}), and the T_d-symmetry isomer of pentamantane, $C_{26}H_{32}$. Our studies show that the T_d center and near C_{2v} centers can be comprised as endohedral minima. These complexes are more stable for smaller and more highly charged metallic particles. The larger cages are also more stable hosts for guest species. The Coulomb interaction between charged guest species and diamondoid cages affects their electronic properties, and represents a possible approach for engineering their HOMO–LUMO gap. Our studies also show that this phenomenon is more significant in diamondoids than in the corresponding Si nanoparticles. The trends of stability, transferred charges between cages and encapsulated particles, and also HOMO–LUMO gaps are almost independent of the type of diamondoids. These results could be applied in the optical engineering of nanodiamond devices, e.g. for use in UV sensors.

Acknowledgments

We are grateful to Dr Neil Drummond for reading the manuscript and providing us with constructive comments. We would also like to thank Professor Arvi Rauk for his helpful advice in constructing orbital interaction diagrams.

References

[1] Mansoori G A 2007 *Adv. Chem. Phys.* **136** 207–58
[2] van Buuren T, Dinh L N, Chase L L, Siekhaus W J and Terminello L J 1998 *Phys. Rev. Lett.* **80** 3803
[3] Bostedt C *et al* 2004 *Appl. Phys. Lett.* **84** 4056
[4] Raty J Y, Galli G, Bostedt C, van Buuren T W and Terminello L J 2003 *Phys. Rev. Lett.* **90** 037401
[5] McIntosh G C, Yoon M, Berber S and Tománek D 2004 *Phys. Rev.* B **70** 045401
[6] Lu A J, Pan B C and Han J G 2005 *Phys. Rev.* B **72** 035447
[7] Drummond N D, Williamson A J, Needs R J and Galli G 2005 *Phys. Rev. Lett.* **95** 096801
[8] Willey T M *et al* 2005 *Phys. Rev. Lett.* **95** 113401
[9] Willey T M *et al* 2006 *Phys. Rev.* B **74** 205432
[10] Xue Y and Mansoori G A 2008 *Int. J. Nanosci.* **7** 63
[11] Kumar V 2004 *Comput. Mater. Sci.* **30** 260
[12] Pichierri F, Kumar V and Kawazoe Y 2005 *Chem. Phys. Lett.* **406** 341
[13] Zhang C-Y, Wu H-S and Jiao H 2005 *Chem. Phys. Lett.* **410** 457
[14] Pichierri F 2006 *Chem. Phys. Lett.* **421** 319
[15] Becke A D 1993 *J. Chem. Phys.* **98** 5648
[16] Lee C, Yang W and Parr R G 1988 *Phys. Rev.* B **37** 785
[17] Williamson A J, Grossman J C, Hood R Q, Puzder A and Galli G 2002 *Phys. Rev. Lett.* **89** 196803
[18] Marsusi F, Mirabbaszadeh K and Mansoori G A 2009 *Physica* E at press (doi:10.1016/j.physe.2008.12.021)
[19] Ditchfield G R, Hehre W J and Pople J A 1971 *J. Chem. Phys.* **54** 724
Hehre W J, Ditchfield R and Pople J A 1972 *J. Chem. Phys.* **56** 2257
[20] Glendening E D, Reed A E, Carpenter J E and Weinhold F 1993 *NBO, Version 3.1* (University of Wisconsin: Madison)
[21] Frisch M J *et al* 1998 *Gaussian 98, Revision A.7* (Pittsburgh, PA: Gaussian, Inc.)
[22] Moran D *et al* 2003 *J. Am. Chem. Soc.* **125** 1142